

Green Chemistry

Accepted Manuscript



This is an *Accepted Manuscript*, which has been through the Royal Society of Chemistry peer review process and has been accepted for publication.

Accepted Manuscripts are published online shortly after acceptance, before technical editing, formatting and proof reading. Using this free service, authors can make their results available to the community, in citable form, before we publish the edited article. We will replace this *Accepted Manuscript* with the edited and formatted *Advance Article* as soon as it is available.

You can find more information about *Accepted Manuscripts* in the [Information for Authors](#).

Please note that technical editing may introduce minor changes to the text and/or graphics, which may alter content. The journal's standard [Terms & Conditions](#) and the [Ethical guidelines](#) still apply. In no event shall the Royal Society of Chemistry be held responsible for any errors or omissions in this *Accepted Manuscript* or any consequences arising from the use of any information it contains.



www.rsc.org/greenchem

ARTICLE

Highly efficient visible-light-driven photoelectrocatalytic selective aerobic oxidation of biomass alcohols to aldehydes

Cite this: DOI: 10.1039/x0xx00000x

Received 00th January 2014,

Accepted 00th January 2014

DOI: 10.1039/x0xx00000x

www.rsc.org/

Yajun Zhang, Guohua Zhao*, Yanan Zhang, Xiaofeng Huang

A green and highly efficient visible-light-driven synergistic photoelectrochemical (PEC) catalysis system was systematically demonstrated for selective oxidation of biomass alcohols to corresponding aldehydes at O₂ atmosphere under the mild condition by employing the Au/CeO₂-TiO₂ NTs as photocathode. Results showed that the conversion of benzyl alcohols was as high as 98% and the selectivity of benzaldehyde > 99% at the bias potential of -0.8 V under the visible light irradiation for 8h. The superior performance could be attributed to the synergistic PEC process combining both the advantages of photocatalytic and electrocatalytic activity. Furthermore, the research elucidated that the PEC activity and the conversion rate of benzyl alcohol could be effectively promoted by adjusting potential. Interestingly, the incorporation of CeO₂ nanoparticles (NPs) into the inner wall of TiO₂ NTs can remarkably enhance the selectivity of the PEC oxidation reaction towards a specific direction. Additionally, the rational designed and fabricated Au/CeO₂-TiO₂ NTs photocathode was in favour of separating electrons and holes. A probable mechanism for the PEC selective aerobic oxidation process was proposed and discussed.

1. Introduction

The selective oxidation of biomass alcohols to corresponding aldehydes under relatively mild condition is one of the most important chemical reactions in the fine chemical, pharmaceutical and agrochemical realm.¹⁻⁶ Traditionally, various oxidants, such as toxic metal oxides, peroxides, halides and ozone etc., were used for these selective catalytic oxidation reaction.^{7,8} Although this type of oxidation reaction could be achieved with high selectivity and high conversion, these reagents are commonly expensive and could cause serious toxicity issues. Additionally, large amounts of reduced residues of the oxidants could potentially lead to environmental pollution.⁹ Compared with the traditional oxidation method, photocatalytic oxidation reaction is considered as a green and highly efficient chemical method that possesses strong oxidation ability under the mild conditions.¹⁰ However, the non-selective nature of photo-induced holes and active oxygen species (e.g., hydroxyl radicals) on the irradiated semiconductor photocatalysts has limited its widespread applications.^{11,12} Consequently, great efforts have been made in the burgeoning research to improve the selectivity of photocatalysis technique.¹³⁻¹⁷

In recent years, Zhao and co-workers² firstly demonstrated the selective photocatalytic oxidation of alcohols with a visible dye-sensitized TiO₂ photocatalyst system when nitroxyl radical TEMPO

was employed as an electron donor. Their subsequent works^{3,4} have extended to use oxygen atom transferred from molecular oxygen on TiO₂ for selective catalytic oxidation in a benzotrifluoride solvent under the UV-light irradiation. The selectivity and conversion have been improved by using molecular oxygen and visible light, which could avoid the generation of strong, non-selective oxidant hydroxyl radicals and photogenerated holes in the photocatalytic process.^{2,6} However, the initial photocatalytic conversion obtained was only about 10~50%. The use of UV light as driving force or large amount of organic solvent in the reaction system could not meet the requirement of green chemistry. Furthermore, TiO₂ powder suspension system commonly adopted in various studies, would lead to the complicated and uneconomical catalysts separation process.^{2,18-20} Nowadays, the research works has been focused on the development of novel photocatalysts possessing superior photocatalytic activity and high reusability to achieve the green and efficient photocatalytic selective oxidation process. As we all know, the electrochemistry as another green catalytic method in catalytic fields has been widely investigated, in which the conversion of final product can be controlled by adjusting the potential.²¹ The integration of electrochemical catalysis with photocatalysis generates unique synergistic PEC catalytic, which could be highly effective in catalytic oxidation. Compared with sole electrocatalysis (EC) and photocatalysis (PC), PEC possesses three advantages: (1) the photocatalysts materials were immobilized on the surface of the

substrate electrode, which could be conveniently separated from the catalytic system. (2) The conversion of biomass alcohols in catalytic reaction could be effectively controlled by adjusting the potential. (3) The synergistic PEC catalysis promotes the catalytic oxidation process for the specific direction with high selectivity. A few works involving PEC selective aerobic oxidation under the visible-light irradiation under mild condition have recently been reported.⁹

The fast-growing research upon TiO₂ composite semiconductor materials offered some unique property (high surface area, thermal stability and chemical stability, etc.) as a new type of visible light driven photocatalyst for water and air treatment to eliminate toxic and recalcitrant organic compounds.²²⁻²⁵ Among those photocatalysts, CeO₂-TiO₂ composite semiconductor has attracted increasing attention due to the unique redox property of CeO₂, which can effectively enhance the visible absorption and photocatalytic activity.^{26,27} Furthermore, the noble metal and its alloy play a vital role in the catalytic field, especially in selective aerobic catalytic oxidation.²⁸⁻³¹ Therefore, various semiconductor and noble metal composite photocatalysts and photoelectrocatalysts, such as Au/TiO₂¹⁹, Pt-Au/TiO₂²⁰ and Au/CeO₂^{9,32} etc. were widely used in catalytic oxidation process. Tanaka and co-worker⁹ found that Au NPs (d_{Au}=13-70 nm) loaded on the CeO₂ (Au/CeO₂) with surface plasmon resonance (SPR) property were more efficient than Au/MO_x (metal oxides) photocatalyst in selective aerobic oxidation of benzyl alcohols. As a result, it is presumed that the key for selective oxidation biomass alcohols is to design and construction of Au/CeO₂-TiO₂ NTs photoelectric integrated electrode with the unique properties of semiconductor and noble metal (high stability, proper redox potential and surface plasmon resonance property).

Herein, based on Au/CeO₂-TiO₂ NTs photocathode, we present a PEC catalytic method for green and highly efficient selective aerobic oxidation of biomass alcohols to aldehydes under visible light irradiation under the mild condition. The electrochemical deposition method was applied to modify TiO₂ NTs with nano-sized CeO₂ NPs, which was beneficial for controlling the morphology, size and quality of nanoparticles, forming the CeO₂-TiO₂ NTs. Moreover, Au NPs was deposited on CeO₂-TiO₂ NTs substrate electrode via photocatalytic reduction method. The PEC performance of the CeO₂-TiO₂ NTs and Au/CeO₂-TiO₂ NTs was systematically investigated. Further experiments clearly demonstrated that the high photocatalytic activity facilitated the catalytic reaction toward a specific direction and the conversion could be efficiently controlled by adjusting the potential. The correlated mechanisms of photoelectrocatalytic aerobic oxidation of benzyl alcohol under visible light irradiation were proposed. This work opens a new doorway to achieve green and highly efficient visible-light-driven photoelectrocatalysis in selective aerobic oxidation under the mild condition.

2. Experiment section

2.1 Chemical Reagents

Pure titanium sheets (99.9 % purity, 1 mm) were cut into 1.5 × 5.0 cm² pieces (actual working area of 1.5 × 2 cm²) and used for electrochemical anodic oxidation. Cerium chloride heptahydrate (CeCl₃·7H₂O), benzyl alcohol and benzaldehyde were all obtained from Sinopharm Chemical Reagent Co.,Ltd., SCRC, China and Chloroauric acid tetrahydrate (HAuCl₄·4H₂O) was purchased from Adamas Reagent, Ltd., Shanghai, China. All the reagents were analytical grade and used without further purification. Deionized water used in the synthesis was from local sources.

2.2 Electrochemical deposition and rapid annealing treatment for preparing CeO₂-TiO₂ NTs substrate electrodes

TiO₂ NTs was prepared by the electrochemical anodic oxidation method according to the literature.³³ (Please see the detailed preparation procedure of TiO₂ NTs in the supplementary information). The deposition of CeO₂ NPs onto TiO₂ NTs was achieved using the electrochemical deposition process.³⁴ Prior to deposition, TiO₂ NTs were immersed in the deposition solution (0.1 mol L⁻¹ CeCl₃ ethanol solution) for 1 h so that the plating solution could diffuse into the TiO₂ NTs. Then the electrochemical deposition was performed at -10 V (vs. SCE) for 10 s (the optimum quality was about 1.6943 g m⁻²) with TiO₂ NTs serving as the working electrodes in a conventional three-electrode system, and a saturated calomel electrode (SCE) and a Pt foil serving as the reference and counter electrode, respectively. After the electrochemical deposition, the sample electrodes were treated at 450 °C for 30 min in a rapid thermal annealing (RTA) furnace, and then for subsequent use.

2.3 Deposition of Au nanoparticles (NPs) on CeO₂-TiO₂ NTs

Photocatalytic reduction method was used to deposit Au NPs on the CeO₂-TiO₂ NTs substrate electrode.³⁵ The CeO₂-TiO₂ NTs was first soaked in 0.3 mmol L⁻¹ aqueous HAuCl₄ solution for 24 h and then was irradiated with a 300 W Xe lamp for 1 h to reduce the absorbed Au³⁺ to Au⁰ by photocatalysis at the expense of water oxidation. The HAuCl₄ concentration and irradiation time were optimized to fabricate Au NPs was loaded with an average size of 50-80 nm and a SPR absorption peak appeared at around 534 nm. For the purpose of comparison, the Au NPs with a size of about 120 nm were also prepared and deposited on the CeO₂-TiO₂ NTs with a HAuCl₄ concentration of 0.5 mmol L⁻¹ and the same irradiation time. Besides, Au (λ_{534nm})/CeO₂/Ti electrode was prepared with the same method as that of Au (λ_{534nm})/CeO₂/TiO₂ NTs, expect that Ti was used as substrate. (Please see the preparation method of Au (λ_{534nm})/CeO₂/Ti in the supplementary information)

2.4 Characterization methods

The chemical compositions of the prepared CeO₂-TiO₂ NTs and Au/CeO₂-TiO₂ NTs electrodes were determined by X-ray photoelectron spectroscopy (XPS, AXIS Ultra HSA, Kratos Analytical Ltd., UK) under ultrahigh vacuum (< 10⁻⁸ torr) using a monochromatic Al Kα X-ray source operating at 150 W. The morphologies of the sample electrodes were characterized by field emission scanning electron microscope (FESEM, Hitach S-4800, Japan). Detailed microstructural features of the sample electrodes were investigated

by high resolution transmission electron microscopy (HR-TEM, JEM2100, JEOL, Japan), using a JEM-2000EX electron microscope operated at 200 kV. Selected-area electron diffraction (SAED) and HR-TEM were applied to identify the crystal structure and to investigate the atomic-scale microstructure of sample electrodes, respectively. The crystalline structure of the samples was analysed by X-ray diffraction (XRD, D8 Focus X-ray diffractometer, Bruker, Germany), using Cu K α radiation ($\lambda = 1.540598 \text{ \AA}$). The components of materials were measured by a Thermo satellite 5000 FT-IR instrument. Raman spectra were obtained on Renishaw inVia Raman Microscope and a 50 \times long working distance objective to focus the laser beam $\lambda = 514 \text{ nm}$. A silicon wafer was used to calibrate the spectrometer at a Raman band of $520 \pm 0.5 \text{ cm}^{-1}$. The UV-vis diffuse reflectance absorption spectra (UV-vis DRS) were recorded using an Avalight-DHS UV-Vis absorbance measurement (Avantes, Netherlands). Digital photos were all take by a FUJIFILM F-60.

2.5 Photoelectrocatalytic performance measurements

All electrochemical and PEC measurements were carried out in a three-electrode cell system of CHI 660c electrochemical workstation. A saturated calomel electrode (SCE) and a Pt foil were served as the reference electrode and the counter electrode, respectively. Electrochemical impedance spectroscopy (EIS) was used to determine the conductivity of as-prepared sample electrodes, with the frequency ranged from 1×10^5 to $1 \times 10^{-3} \text{ Hz}$, and the amplitude was 5 mV. The electrolyte was 0.1 mol L^{-1} KCl aqueous solution containing 0.05 mol L^{-1} $[\text{Fe}(\text{CN})_6]^{3-}/[\text{Fe}(\text{CN})_6]^{4-}$. Photocurrent density was measured in 0.1 mol L^{-1} Na_2SO_4 solution. To evaluate the PEC performance, PEC selective aerobic oxidation experiment was carried out in a three electrodes cell system. The volume of electrolyte was 100 mL consisting of 1 mmol L^{-1} benzyl alcohol and 0.1 mol L^{-1} Na_2SO_4 . The electrolyte was purged with O_2 for 30 min to remove N_2 and other impurity gases prior to the experiment. A 300 W PSL-SXF300 high-pressure short-arc xenon lamp (Changtuo, China) served as the visible light source (wavelength of 420–800 nm,

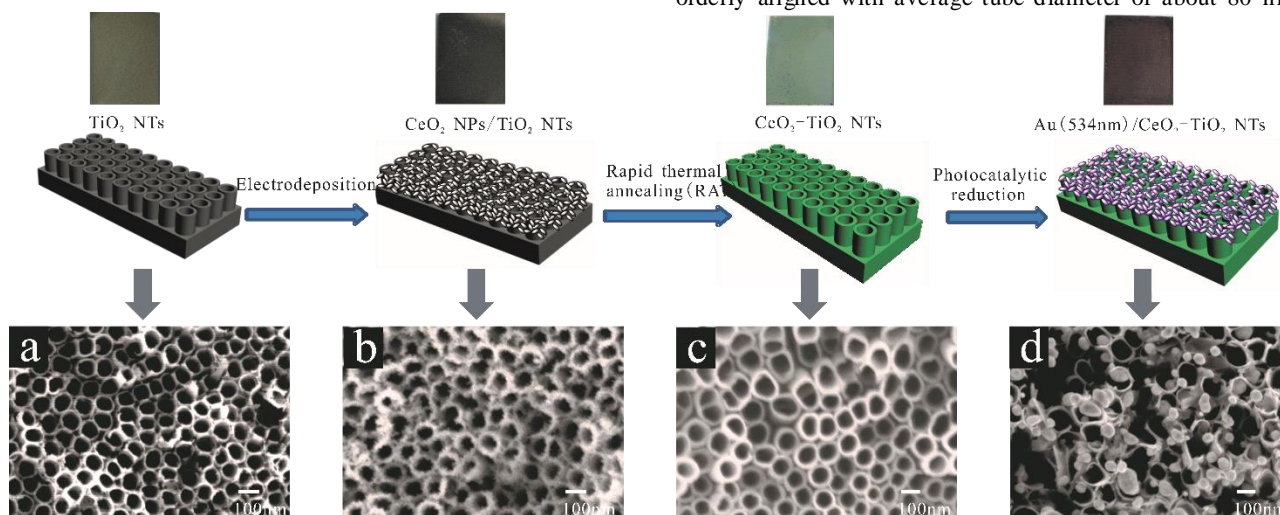
light intensity of 100 mW cm^{-2}). The identification of the oxidation products of the benzyl alcohols was conducted on the GC-MS (Agilent 6890/5973 N, Agilent Co.) and the conversion of benzyl alcohols and the formation of benzaldehyde was measured by HPLC (Agilent 1260, Agilent Co.) equipped with an Eclipse Plus C18 ($4.6 \times 100 \text{ mm}$, $3.5 \mu\text{m}$) and the selected UV detector at $\lambda = 254 \text{ nm}$. A 48:52 (v:v) methanol/ H_2O was employed as the mobile phase at the flow rate of 1 mL min^{-1} .

3. Results and discussion

3.1 Construction and PEC performance of the visible-light-driven photoelectric integrated cathode

3.1.1 Synthesis and PEC performance of one-dimensional CeO_2 - TiO_2 NTs substrate electrode

Scheme.1 presents the design and fabrication strategy of the Au/ CeO_2 - TiO_2 NTs photoelectrode. The detailed synthesis and experimental process could be found in the experiment section. Briefly, the CeO_2 nanoparticles (CeO_2 NPs) were deposited onto the TiO_2 NTs via electrochemical deposition method, forming the CeO_2 - TiO_2 composite nanotubes (CeO_2 - TiO_2 NTs) substrate electrodes; finally, Au NPs was deposited onto the CeO_2 - TiO_2 NTs by a facile photocatalytic reduction deposition method. It was worth mentioning that Au NPs with different sizes showed distinct SPR absorption. In this work, the Au NPs were denoted as the Au ($\lambda_{534 \text{ nm}}$) and Au ($\lambda_{480 \text{ nm}}$) etc., where the subscripts '534 nm' or '480 nm' corresponded to the SPR absorption of Au/ CeO_2 - TiO_2 NTs in the UV diffuse reflection spectroscopy (UV-DRS). The digital photos at the top inset in Scheme.1 clearly showed variations of visual colour on the surface of sample electrode, providing a macroscopic evidence for the variations of optical properties. At the bottom of inset in Scheme.1, the field emission scanning electron microscope (FE-SEM) morphologies of as-prepared sample electrodes were presented. The as-prepared uniform TiO_2 NTs array were highly orderly aligned with average tube diameter of about 80 nm and



Scheme.1 Schematic illustration of the preparation of the Au/ CeO_2 - TiO_2 NTs photocathode

very thin wall of less than 10 nm in thickness (Scheme.1a). The nano-sized CeO₂ NPs were uniform deposited onto the top of TiO₂ NTs, which improved the absorption of visible light effectively. After the treatment of RTA, the macroscopic colour of the electrode surface changed from black to green, and the CeO₂ NPs disappeared in the SEM image, indicating that the CeO₂ NPs may dope into the wall of TiO₂ NTs, forming CeO₂-TiO₂ NTs (Scheme.1c). The Au NPs were subsequently deposited onto the CeO₂-TiO₂ NTs, which was judiciously chosen to further increase the visible light absorption of CeO₂-TiO₂ NTs employing the surface plasmon resonance properties. Therefore, the superior photoelectrocatalytic activity and excellent PEC performance of the Au/CeO₂-TiO₂ NTs photoelectrode for selective oxidation of biomass alcohols can be expected.

To investigate the optical absorption property, the UV-DRS of pure TiO₂ NTs and CeO₂-TiO₂ NTs was recorded and presented in Fig.1a. In UV region, TiO₂ NTs presented a continuous absorption band from 200 to 385 nm, corresponding to 3.22 eV band gap. As for the CeO₂-TiO₂ NTs, not only a red shift of the band gap absorption edge (385 to 500 nm) was observed, but also the absorption were significantly enhanced in the visible region, suggesting the successful deposition of CeO₂ into the TiO₂ NTs. The photocurrent response of the CeO₂-TiO₂ NTs electrode under visible light (420-800 nm) irradiation was compared with that of the pure TiO₂ NTs electrode. Fig.1b illustrated the linear sweeping voltammograms (LSVs) of as-prepared sample electrodes. Notably, the photocurrent response of CeO₂-TiO₂ NTs dramatically increased after -0.4 V (vs. SCE). However, the LSVs of TiO₂ NTs was almost negligible under the same condition. The enhanced photocurrent density of the CeO₂-TiO₂ NTs was due to the modification of the narrow-band semiconductor CeO₂ NPs, which had extended the absorption of TiO₂ NTs to visible region. Meanwhile, the heterojunction formed between two semiconductors facilitated the separation of photogenerated electrons and holes. In addition, taken on the photo-to-current conversion efficiency (η , PCE) Eq. [1], the maximum value for TiO₂ NTs and CeO₂-TiO₂ NTs could be calculated using the following equation³⁶:

$$\eta(\%) = \frac{j_p \times (E_{rev} - |E_{app}|)}{I_0} \times 100 \quad [1]$$

Where j_p (mA cm⁻²) is the photocurrent density, $j_p \times E_{rev}$ is the total power output, $j_p \times |E_{app}|$ is the electrical power input, I_0 (mW cm⁻²) is the power density of the incident light, E_{rev} is the standard reversible potential (1.23 V for the water splitting reaction at pH = 0) and $|E_{app}|$ is the absolute value of the applied potential (which is obtained as $E_{app} = E_{means} - E_{ocp}$, where E_{means} is the electrode potential of the electrode potential of the working electrode when j_p is measured under irradiation, and E_{ocp} is the applied potential at the open circuit under the same conditions). The photo-to-current conversion efficiency vs. applied bias potential was plotted in Fig.1b (inset). The value of η could be optimized for the different amount of CeO₂ loaded on the TiO₂ NTs (Supporting Information, SI-Fig.1) and the

maximum η of TiO₂ NTs and CeO₂-TiO₂ NTs were achieved as 0.58% and 2.8% at bias potential of -0.8 V, respectively. Chronoamperometric $i-t$ curves of pure TiO₂ NTs and CeO₂-TiO₂ NTs at bias potential of -0.8 V under periodical visible light irradiation ($\lambda > 420$ nm) was also recorded (Fig. 1c). Compared to the photocurrent densities of -0.015 mA cm⁻² for TiO₂ NTs, the average value of photocurrent densities of CeO₂-TiO₂ NTs reached -0.09 mA cm⁻² and was very stable even after 5 periods. It further indicated durable photocurrent response stability, anti-photocorrosion and distinguished PEC activity of CeO₂-TiO₂ NTs.

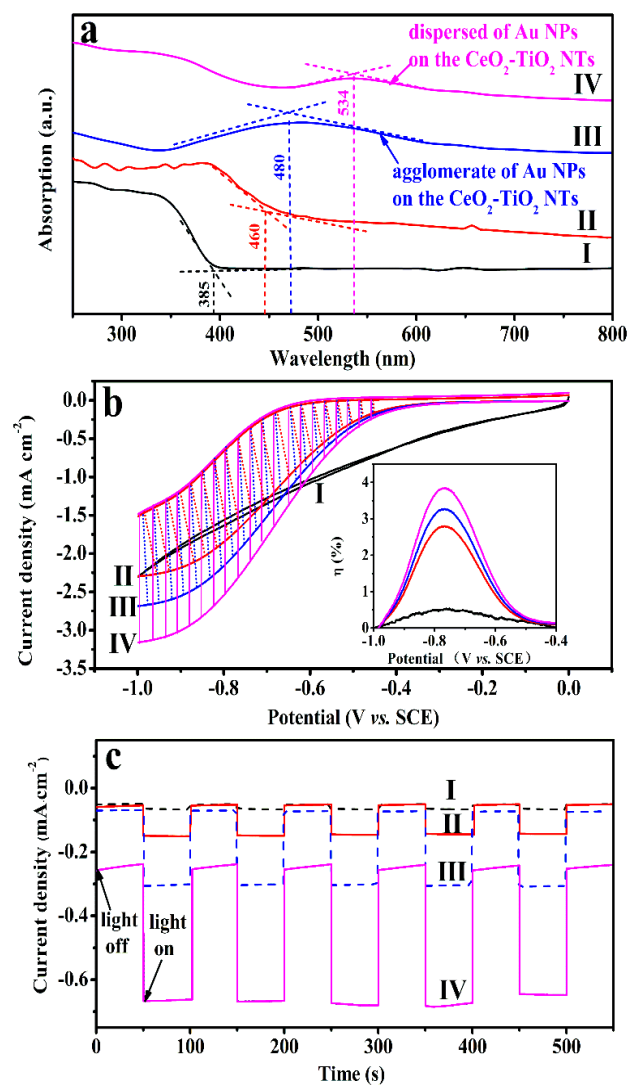


Fig.1 a: UV-DRS, b: LSVs in 0.1 mol L⁻¹ Na₂SO₄ at the scan rate of 100 mV S⁻¹ (insert: PCE curves) and c: Chronoamperometric $i-t$ curves in 0.1 mol L⁻¹ Na₂SO₄ at -0.8 V (vs. SCE) with periodical visible light irradiation (interval of 50s) of different photocathodes (I: pure TiO₂ NTs, II: CeO₂-TiO₂ NTs, III: Au ($\lambda_{480\text{nm}}$)/CeO₂-TiO₂ NTs and IV: Au ($\lambda_{534\text{nm}}$)/CeO₂-TiO₂ NTs).

The excellent PEC performance of the CeO₂-TiO₂ NTs electrode was resulted from its structural characteristics and unique optical

property. The TEM images and the diffraction pattern of the TiO₂ NTs before and after deposition of the CeO₂ NPs were illustrated in Fig.2a and Fig.2b, respectively. The HR-TEM image (Fig. 2b) of the CeO₂-TiO₂ NTs exhibited the composite nanotubes with a uniform and micro-porous structure of inner wall, in which the lattice fringe of 0.35 nm, 0.312 nm and 0.614 nm were indexed to the reflections from the (101), (111) and (002) crystallographic plane of TiO₂, CeO₂ and Ti₂O₇, respectively. In addition, it was found that the CeO₂ NPs doped into the TiO₂ NTs disappeared. As shown in Fig.2a and Fig.2b, the diffraction rings of the selected area electron diffraction (SAED) pattern in the inset further affirmed the good crystallinity of the anatase phase of TiO₂ and ceria. The XRD patterns of the TiO₂ NTs and CeO₂-TiO₂ NTs was shown in SI-Fig.2. The diffraction peaks observed at $2\theta = 25.5^\circ$ and 37.9° were assigned to the (101) and (004) planes of anatase TiO₂, respectively. The diffraction peak at $2\theta = 47.5^\circ$ was assigned to CeO₂ (220). The fluorite cubic phase of CeO₂ and pure anatase phase of TiO₂ were in the composite material, which was in good agreement with the standard data of the JCPDS card. The Raman scattering spectra of TiO₂ NTs and CeO₂-TiO₂ NTs (SI-Fig.3) revealed the three characteristic peaks for anatase phase of TiO₂ (B_{1g} mode at 390 cm⁻¹, A_{1g} mode at 510 cm⁻¹ and E_g mode at 630 cm⁻¹). It was known that the pure CeO₂ have a strong band at 460 cm⁻¹ (F_{2g} mode) attributed to the Raman active mode characteristic of fluorite-structure material.³⁷ The faint of this characteristic peak in the Raman spectrum of CeO₂-TiO₂ NTs confirmed that Ce species co-existed with the Ti species. These Raman principal peak indicated³⁸ that the modification of CeO₂ NPs might increase the number of surface oxygen vacancies or defects in micro-pore inner walls of TiO₂ NTs, which was consistent with the result of HR-TEM (Fig. 2b). Moreover, the FT-IR spectra of as-prepared samples confirmed the result of Raman spectrum and the HR-TEM image of composite nanotubes (SI-Fig. 4).

The chemical composition of TiO₂ NTs and CeO₂-TiO₂ NTs was analysed by X-ray photoelectron spectroscopy (XPS).^{38,39} The peaks corresponding to Ce 3d, O 1s and Ti 2p were clearly shown in Fig.3. The Ce 3d region (Fig. 3a) consisted of three 3d_{3/2}-3d_{5/2} spin-orbit split doublets of 3d core holes and the associate satellites (labelled Ce⁴⁺). The peaks located around $\nu = 882.3$ eV and $\nu = 901.2$ eV could be assigned to the Ce 3d_{5/2} and Ce 3d_{3/2} state of Ce⁴⁺, respectively, with spin-orbit splitting of 18.9 eV. The u''/v'' doublet was due to the primary photoemission from Ce⁴⁺-O₂. The u/v and u''/v'' doublets were shake down features resulting from the transfer of one or two electrons from a filled O 2p orbital to an empty Ce 4f orbital. The u'/v' doublets were due to photoemission from Ce³⁺ cations. Therefore, a mixture of Ce³⁺/Ce⁴⁺ oxidation states exists on the surface of composite nanotube after the RTA treatment process. Meanwhile, the Ti 2p_{3/2} binding energies for CeO₂-TiO₂ (Fig. 3b) was 458.3 eV, which was characteristic of Ti⁴⁺ in TiO₂ (458.6 eV).²⁶ This result indicated the Ce atom in the composite nanotube showed no significant influence on the XPS spectra of either the Ti 2p level or the O 1s level, indicating that Ce had not entered into the lattices of TiO₂. Nevertheless, it was worthy to note that the doping of CeO₂ into TiO₂ generated more adsorption oxygen on the surface. The O 1s region (Fig.3c) was fitted into

two sub-bands, which at the lower binding energy of the sub-bands corresponded to the lattice oxygen O²⁻ (denoted as O_β), and that at higher binding energy of the sub-bands corresponded to the surface adsorbed oxygen (denoted as O_α), such as O₂²⁻ or O⁻ belonging to defect-oxide or hydroxyl-like group. The O_α ratio on CeO₂-TiO₂ NTs (21.8%) calculated by O_α/(O_α + O_β) was much higher than that of pure TiO₂ NTs (13.8%). The higher ratio meant the synergistic effect between Ce and Ti species and resulted in more surface oxygen vacancies. Usually, O_α was more active than O_β in oxidation reduction reactions (ORR) due to its higher mobility.³⁸ Therefore, the higher O_α ratio on CeO₂-TiO₂ NTs was beneficial for the O₂ reduction to •O₂⁻ radicals in the ORR, and thereby facilitated PEC selective aerobic oxidation and enhanced the conversion at mild condition. As shown in Fig.3d, the semi quantitative analysis of element content of preparing TiO₂ NTs and CeO₂-TiO₂ NTs were investigated.

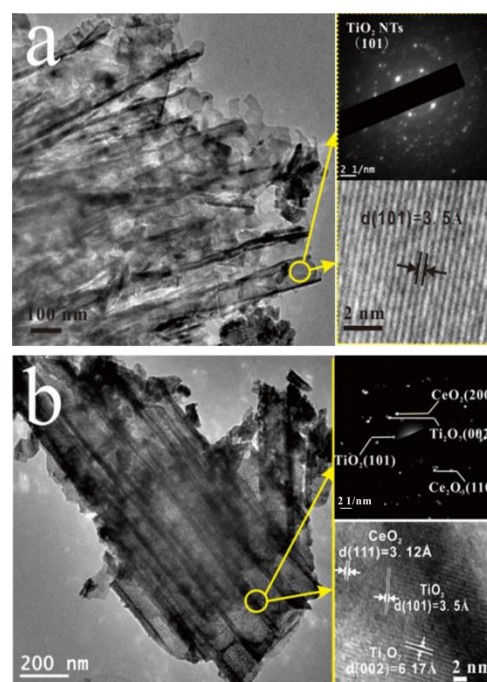


Fig.2 TEM image, HR-TEM image and SAED pattern of pure TiO₂ NTs (a) and CeO₂-TiO₂ NTs (b)

3.1.2 Modification of CeO₂-TiO₂ NTs with Au NPs

A facile photocatalytic reduction method was employed in this paper to obtain the nano-sized Au particles on the CeO₂-TiO₂ NTs electrode. Details on the structural characteristic and PEC performance of Au/CeO₂-TiO₂ NTs were investigated. The UV-DRS of Au/CeO₂-TiO₂ NTs electrode in Fig.1a showed the enhanced visible light absorption in the visible range. Compared with the SPR absorption around 534 nm (~60 nm, SEM image in Fig.4a) of Au NPs, the Au NPs with a larger size (~120 nm, SEM image in SI-Fig.5) on the CeO₂-TiO₂ NTs depicted a blue shift of SPR peak at 480 nm. The significant visible light enhancement around 534 nm on the as-prepared Au/CeO₂-TiO₂ NTs was due to the SPR absorption

of Au NPs at this wavelength, which was in good agreement with the measured SPR wavelength of 558 nm of the same-sized Au particles dispersed in solution.³⁵

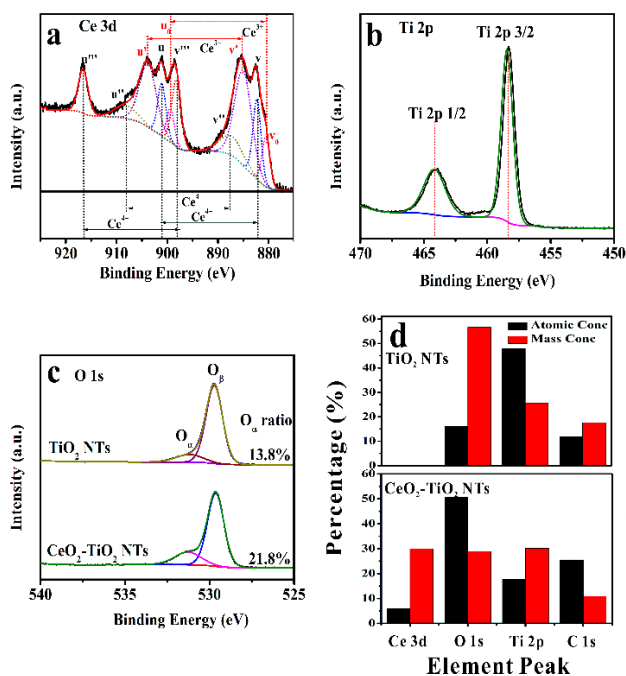


Fig.3 XPS spectra of Ce 3d (a), Ti 2p (b), O1s (c) and elemental analysis (d) on preparing sample electrodes.

PEC properties of Au ($\lambda_{480\text{nm}}$)/CeO₂-TiO₂ and Au ($\lambda_{534\text{nm}}$)/CeO₂-TiO₂ electrodes were evaluated. The LSV curves of different sample electrodes were measured under visible light irradiation and shown in Fig.1b. Compared with CeO₂-TiO₂ NTs and TiO₂ NTs electrodes, the enhanced photocurrent density observed on Au NPs modified CeO₂-TiO₂ NTs electrodes were indicative of improved charge separation in the Schottky junction between semiconductor and noble metal. From Fig.1b, it was found that the photocurrent density of Au ($\lambda_{480\text{nm}}$)/CeO₂-TiO₂ NTs was smaller than that of Au ($\lambda_{534\text{nm}}$)/CeO₂-TiO₂ NTs. Results showed that the contribution of Au particles with bigger size to photocurrent density was small. The maximum PCE value of Au ($\lambda_{534\text{nm}}$)/CeO₂-TiO₂ NTs electrode was calculated using Eq.[1]. It reached 4 %, which had an improvement of 6.89, 1.42 and 1.25 times over pure TiO₂ NTs, CeO₂-TiO₂ NTs and Au ($\lambda_{480\text{nm}}$)/CeO₂-TiO₂ NTs, respectively. Results clearly showed that the superior PEC activity on the Au ($\lambda_{534\text{nm}}$)/CeO₂-TiO₂ NTs electrode was expected. The measurement condition for photocurrent responses of Au ($\lambda_{480\text{nm}}$)/CeO₂-TiO₂ and Au ($\lambda_{534\text{nm}}$)/CeO₂-TiO₂ NTs electrode were the same as that of CeO₂-TiO₂ NTs electrode. Compared with the photocurrent density of CeO₂-TiO₂ NTs (-0.09 mA cm⁻²), the average value of photocurrent densities on the Au ($\lambda_{480\text{nm}}$)/CeO₂-TiO₂ and Au ($\lambda_{534\text{nm}}$)/CeO₂-TiO₂ NTs electrode reached -0.24 and -0.44 mA cm⁻², respectively. The microstructure characteristics of Au ($\lambda_{534\text{nm}}$)/CeO₂-TiO₂ NTs electrode were characterized. The FE-SEM image of the Au/CeO₂-TiO₂ NTs photocathode was presented in Fig.4a, which clearly exhibited the morphology of Au NPs with a mean size of around 50-

80 nm in Fig.4b. As shown in SI-Fig.6, the elemental mapping for the debris of the Au ($\lambda_{534\text{nm}}$)/CeO₂-TiO₂ NTs was another evidence for the successful deposition Au on the CeO₂-TiO₂ NTs. In the case of the debris, some Au particles displayed irregular scattered points, which showed good agreement with a small particle portion detected. Further morphological feature of Au ($\lambda_{534\text{nm}}$)/CeO₂-TiO₂ NTs was carried out by TEM in Fig.4c. The TEM image of Au ($\lambda_{534\text{nm}}$)/CeO₂-TiO₂ NTs exhibited the higher density and smaller size of Au NPs onto the CeO₂-TiO₂ NTs. The XRD patterns of Au ($\lambda_{534\text{nm}}$)/CeO₂-TiO₂ NTs showed the dominant Au peak that could be indexed to the (200) and (220) plane (SI-Fig.7). The XPS spectra of Au ($\lambda_{534\text{nm}}$)/CeO₂-TiO₂ NTs were presented in Fig.4d. The Au 4f region consisted of two asymmetric peaks was assigned to 4f_{5/2} and 4f_{7/2} core levels. The Au 4f_{7/2} core level could be fitted with a single peak at a binding energy of 80.8 eV, which was attributed to metallic gold Au⁰.³⁵ A significant negative shift (ca.3.2 eV) of the binding energy for Au 4f_{7/2} relative to 84.0 eV of the bulk Au was identified, which was due to the electron transfer from oxygen vacancies of the CeO₂-TiO₂ NTs to Au, leading to a lower Au 4f_{7/2} core level binding energy in the Au ($\lambda_{534\text{nm}}$)/CeO₂-TiO₂ NTs.³⁵

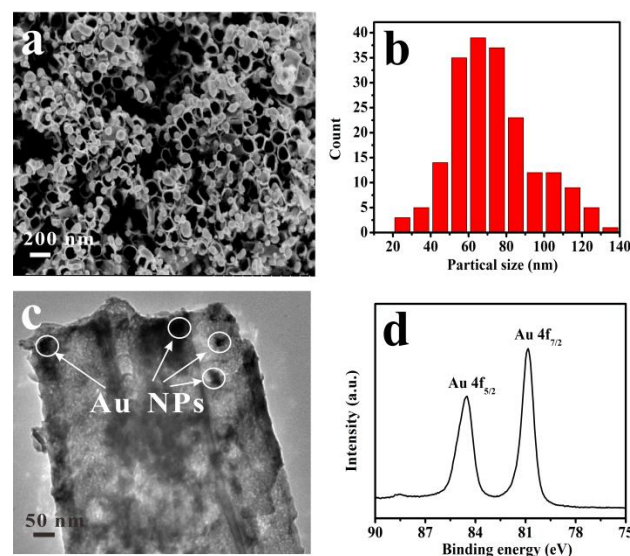


Fig.4 SEM image (a); Au particles size distribution (b); TEM and HRTEM image (c) and XPS spectra of Au ($\lambda_{534\text{nm}}$)/CeO₂-TiO₂ NTs (d).

The interfacial properties between the electrode and the electrolyte were scrutinized by electrochemical impedance spectroscopy (EIS) measurements. A semicircle (i.e., the arch in the present study) in the Nyquist plot at high frequency represented the charge-transfer process, while the diameter of the semicircle reflected the charge-transfer resistance (Fig.5).⁴⁰ Fig.5a presented the EIS of Au ($\lambda_{534\text{nm}}$)/CeO₂-TiO₂ NTs electrode, CeO₂-TiO₂ NTs electrode and TiO₂ NTs electrode in 0.1 mol L⁻¹ KCl solution containing 0.05 mol L⁻¹ [Fe(CN)₆]³⁻/[Fe(CN)₆]⁴⁻. In the frequency range of 1×10^5 to 1×10^3 Hz, the smaller Faraday resistance was observed in Au ($\lambda_{534\text{nm}}$)/CeO₂-TiO₂ NTs electrode, indicating a faster electron transfer rate in the surface electrochemical process. The interfacial

PEC properties of the Au ($\lambda_{534\text{nm}}$)/CeO₂-TiO₂ NTs electrode was further investigated in 0.1 mol L⁻¹ Na₂SO₄ solution under visible light irradiation (Fig.5b). Clearly, the arches for Au ($\lambda_{534\text{nm}}$)/CeO₂-TiO₂ NTs electrode under the visible light irradiation was smaller than that recorded in dark condition, implying that the Au NPs deposited significantly enhanced the electron mobility by reducing the recombination of electron-hole pairs.

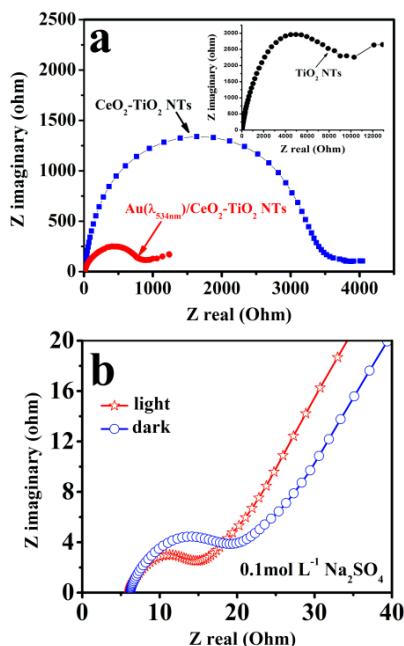


Fig.5 Nyquist plot of as-prepared electrodes (a) and Au ($\lambda_{534\text{nm}}$)/CeO₂-TiO₂ NTs with light on/off (b) in 0.1 mol L⁻¹ KCl containing 0.05 mol L⁻¹ [Fe(CN)₆]³⁻/[Fe(CN)₆]⁴⁻ and 0.1 mol L⁻¹

Na₂SO₄ solution, respectively.

3.2 Selective PEC aerobic oxidation of benzyl alcohols under the visible light irradiation at the mild condition

Based on that mentioned above, the superior PEC performance of Au ($\lambda_{534\text{nm}}$)/CeO₂-TiO₂ NTs electrode was systematically investigated in selective PEC aerobic oxidation of benzyl alcohol, which was always served as a probe reagent of biomass alcohol under visible light irradiation at mild condition with O₂ atmosphere.

The experiment was conducted in 0.1 mol L⁻¹ Na₂SO₄ solution containing 0.1 mmol L⁻¹ benzyl alcohols (100 ml) at the O₂ atmosphere under the mild condition. It was found that the final product detected in the liquid phase was mainly benzaldehyde via GC-MS. It indicated that the prepared Au ($\lambda_{534\text{nm}}$)/CeO₂-TiO₂ NTs photocathode exhibited superior selectivity in the PEC aerobic oxidation of benzyl alcohols. As shown in the Table.1, the effect of different bias potential was investigated for PEC or EC selective aerobic oxidation of benzyl alcohol on the Au ($\lambda_{534\text{nm}}$)/CeO₂-TiO₂ NTs. Under PEC condition, with the increase of bias potential from -0.5 V to -0.8 V, the conversion of benzyl alcohol continuously increased from 63% to 98%. However, when the bias potential was over -0.8 V to -1 V, the conversion was apparently decreased from 98% to 76%. Compared with the PEC, similar results were obtained in EC process under the bias potential form -0.5 V to -0.8 V, and the conversion of benzyl alcohol increased form 52% to 74%. And with the bias potential increased to -1 V, the conversion was reduced to 56%. Compared with EC process, PEC exhibited highly efficient catalytic activity. Both of the catalytic process had excellent selectivity (> 99%) and the maximum conversion of benzyl alcohols for PEC and EC was achieved at the bias potential of -0.8 V. Such high conversion of benzyl alcohols by PEC and EC methods to benzaldehyde in the present work was easily obtained compared to

Table.1 The effect of different bias potential for PEC or EC selective aerobic oxidation of benzyl alcohols on the Au ($\lambda_{534\text{nm}}$)/CeO₂-TiO₂ NTs (100 mV cm⁻²).

		-500mV				-800mV				-1000mV			
		2h	4h	6h	8h	2h	4h	6h	8h	2h	4h	6h	8h
C _{reactant}	PEC	0.87	0.70	0.55	0.37	0.61	0.32	0.14	0.02	0.76	0.51	0.41	0.24
	EC	0.96	0.84	0.55	0.48	0.85	0.72	0.52	0.26	0.87	0.76	0.61	0.44
C _{product}	PEC	0.13	0.30	0.45	0.63	0.39	0.68	0.86	0.98	0.26	0.49	0.59	0.76
	EC	0.04	0.16	0.45	0.52	0.15	0.28	0.48	0.74	0.13	0.24	0.39	0.56
Conversion	PEC	13%	30%	45%	63%	39%	68%	86%	98%	26%	49%	59%	76%
	EC	4%	16%	45%	52%	15%	28%	48%	74%	13%	24%	39%	56%
Selectivity	PEC	>99%	>99%	>99%	>99%	>99%	>99%	>99%	>99%	>99%	>99%	>99%	>99%
	EC	>99%	>99%	>99%	>99%	>99%	>99%	>99%	>99%	>99%	>99%	>99%	>99%

C., concentration (mol L⁻¹); liquid products were detected using GC-MS and quantified using HPLC

PEC., Photoelectrochemical catalytic; EC., electrochemical catalytic

rigorous conditions, such as UV-light irradiation, or long time (12 h or 20 h) light irradiation adopted in the literature.^{3,9,18,19} Meanwhile, water was used as solvent instead of organic liquid, and it was more promising under the concept of green chemistry. Furthermore, the conversion of benzyl alcohols obtained by PEC in the current study was much higher than that by photocatalysis, which was 10~40% for anatase TiO₂ and 50% for rutile TiO₂ with selectivity of 38%, respectively.^{3,18}

From the Table.1, we also noticed that the formation of benzaldehyde was consistent with the conversion of benzyl alcohol. Therefore, the conversion of benzyl alcohols could be efficiently controlled by adjusting the potential, in which the separation of photogenerated electrons and holes could be regulated. It fully embodied the essential role of the applied potential in the PEC aerobic conversion of benzyl alcohol.

To demonstrate the advantage of nano-sized Au particles on the PEC performance of the Au/CeO₂-TiO₂ NTs electrode, Au particles of different amount and sizes were prepared and deposited on the CeO₂-TiO₂ NTs via photocatalytic reduction method. As shown in Fig.6, Au (λ_{480 nm})/CeO₂-TiO₂ NTs and CeO₂-TiO₂ NTs exhibited much lower PEC activity than Au (λ_{534 nm})/CeO₂-TiO₂ NTs. Under the visible light irradiation for 8h and at the bias potential of -0.8 V, the conversion of benzyl alcohol was only 15% and 52% for pure CeO₂-TiO₂ NTs and Au (λ_{480 nm})/CeO₂-TiO₂ NTs, respectively. This result indicated that modification of nano-sized Au particles could efficiently enhance the PEC activity and the benzyl alcohol conversion owing to the strong SPR absorption at visible region. Herein, the contribution of TiO₂ NTs in selective PEC aerobic oxidation of benzyl alcohol was also investigated. The conversion of benzyl alcohols on Au (λ_{534 nm})/CeO₂/Ti was only 81% compared to that of 98% on Au (λ_{534 nm})/CeO₂-TiO₂ NTs, which suggested that the three-dimensional nano-structure of TiO₂ NTs greatly contributed to PEC aerobic oxidation benzyl alcohols. Usually, TiO₂ NTs does not have visible light response. When CeO₂ and Au nanoparticles were loaded on TiO₂ NTs substrate electrode, heterojunction was formed between CeO₂ and TiO₂ NTs. Besides, the Schottky junction was formed between the noble metal Au and semiconductor CeO₂-TiO₂ NTs. Both aspects could effectively promote the separation of photogenerated electrons and holes and enhance the photoelectrocatalytic activity.

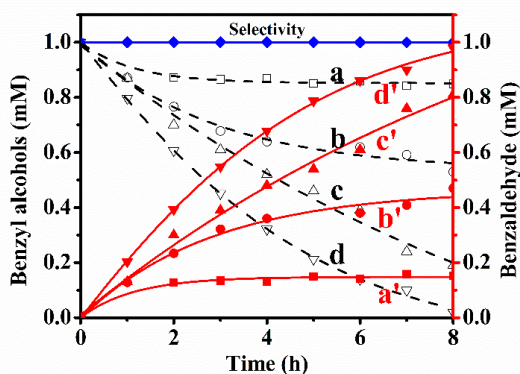


Fig.6 The selective PEC aerobic oxidation of benzyl alcohols and benzaldehyde formation and selectivity for different photocathodes under 100 mW cm⁻² visible light irradiation (a and a': CeO₂-TiO₂ NTs; b and b': Au (λ_{480nm})/CeO₂-TiO₂ NTs; c and c': Au (λ_{534nm})/CeO₂/Ti; d and d': Au (λ_{534nm})/CeO₂-TiO₂ NTs).

Accordingly, a possible reaction mechanism for PEC aerobic oxidation on Au (λ_{534nm})/CeO₂-TiO₂ NTs photocathode was briefly described in Fig.7 and the following equations.^{15,41,42} Under the visible light irradiation, the photogenerated electrons and holes were produced. The adsorbed benzyl alcohol on the surface of the photocathode interacted with holes to produce benzyl alcohol cation radicals Eq.[3]. Whereas, the molecular O₂ was activated by the photoelectrons to form •O₂⁻ radicals Eq.[4]. The formed •O₂⁻ radicals reacted with the benzyl alcohol cation radicals to produce benzaldehyde (Eq.[5]). The nano-sized Au particles would trap the photo-induced electron to prolong the lifetime of charge carriers, improving the efficiency of PEC process. In addition, the bias potential played an important role in adjusting the separation of the holes and electrons and also the amount of the activity species of •O₂⁻ in the oxidation reaction, leading to different conversion rate.

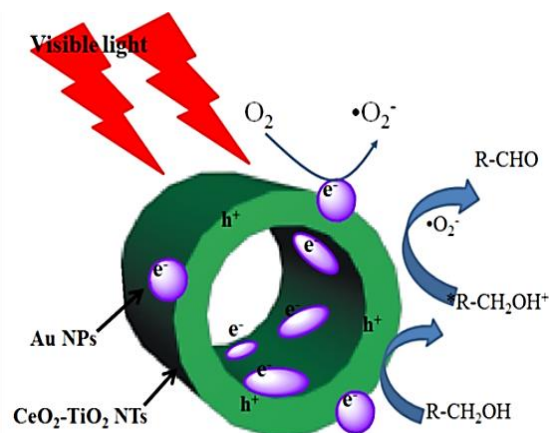
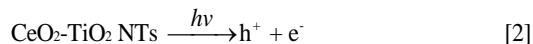


Fig.7 A plausible reaction mechanism of PEC selective aerobic oxidation of benzyl alcohols under visible light irradiation



Finally, the important features for Au/CeO₂-TiO₂ NTs photocathode would be noticed as follows: (1) controllable modification of Au NPs on the CeO₂-TiO₂ NTs photocathode by photocatalytic reduction methods, (2) correlation between structure and PEC activities of Au/CeO₂-TiO₂ NTs photocathode in benzyl alcohol conversion, and (3) selective PEC aerobic oxidation of benzyl alcohol to benzaldehyde under the visible light at the mild condition.

Conclusions

In summary, this work has demonstrated the green and highly efficient selective catalytic oxidation of biomass alcohols via visible-light-driven synergistic PEC on the Au/CeO₂-TiO₂ NTs photocathode at the mild condition. The prepared Au/CeO₂-TiO₂ NTs photocathode exhibited excellent PEC performance for selective aerobic oxidation. In particular, at the bias potential of -0.8 V and visible light irradiation for 8 h, the conversion of benzyl alcohol was 98% and the selectivity of benzaldehyde formation >99% was obtained. Therefore, this work would lead to a new opportunity for visible-light-driven selective PEC aerobic oxidation of biomass alcohols to useful chemicals.

Acknowledgements

This work is supported by the National Natural Science Foundations of China (NSFC, No. 21277099)

Notes and references

*Corresponding Author: Phone: (86)-21-65981180.

Fax: (86)-21-65982287. E-mail: g.zhao@mail.tongji.edu.cn.

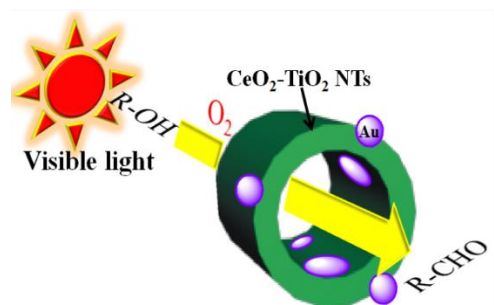
Department of Chemistry, Key Laboratory of Yangtze River Water Environment, Tongji University, Shanghai 200092, People's Republic of China

Electronic Supplementary Information (ESI) available: [Additional the preparation method of TiO₂ NTs and Au (λ_{534nm})/CeO₂/Ti; the PCE of deposited amount CeO₂ NPs; XRD pattern, Raman spectra and FT-IR spectra of TiO₂ NTs and CeO₂-TiO₂ NTs.; SEM image of Au (λ_{480nm})/CeO₂-TiO₂ NTs; the elemental mapping of Au (λ_{534nm})/CeO₂-TiO₂ NTs and XRD pattern of Au/CeO₂-TiO₂ NTs. See DOI: 10.1039/c000000x/

- D. I. Enache, J. K. Edwards, P. Landon, B. S. Espriu, A. F. Careley, A. A. Herzing, M. Watanabe, C. J. Kiely, D. W. Knight and G. J. Hutchings, *Science*, 2006, **311**, 362.
- M. Zhang, C. C. Chen, W. H. Ma and J. C. Zhao, *Angewandte Chemie*, 2008, **120**, 9876.
- M. Zhang, Q. Wang, C. C. Chen, L. Zang, W. H. Ma and J. C. Zhao, *Angewandte Chemie International Edition*, 2009, **48**, 6081.
- Q. Wang, M. Zhang, C. C. C. Chen, W. H. Ma and J. C. Zhao, *Angewandte Chemie International Edition*, 2010, **49**, 7976.
- S. Bawaked, Q. He, N. F. Dummer, A. F. Carley, D. W. Knight, D. Bethell, C. J. Kiely and G. J. Hutchings, *Catalysis Science & Technology*, 2011, **1**, 747.
- X. Y. Xiao, J. Jiang and L. Z. Zhang, *Applied Catalysis B: Environmental*, 2013, **142**, 487.
- G. J. ten Brink, I. W. C. E. Arends and R. A. Sheldon, *Science*, 2000, **287**, 1636.
- P. F. Zhang, Y. T. Gong, H. R. Li, Z. R. Chen and Y. Wang, *Nature communications*, 2013, **4**, 1593.
- A. Tanaka, K. Hashimoto and H. Kominami, *Journal of the American Chemical Society*, 2012, **134**, 14526.
- M. Fujihira, Y. Satoh and T. Osa, *Nature*, 1981, **193**, 206.
- S. N. Chai, G.H. Zhao, Y. N. Zhang, Y. J. Wang, F. Q. Nong, M. L. Li and D. M. Li, *Environmental Science & Technology*, 2012, **46**, 10182.
- Y. N. Zhang, F. Q. Nong, H. J. Shi, S. N. Chai, X. F. Huang, G. H. Zhao, Y. G. Zhang and Y. L. Zhang, *Electrochemistry Communications*, 2013, **33**, 5.
- J. C. Colmenares and R. Luque, *Chemical Society Reviews*, 2014, **43**, 765-778.
- P. F. Zhang, Y. Wang, J. Yao, C. M. Wang, C. Yan, M. Antonietti and H. R. Li, *Advanced Synthesis & Catalysis*, 2011, **353**, 1447-1451.
- J. G. Wang, Z. F. Bian, J. Zhu and H. X. Li, *Journal of Materials Chemistry A*, 2013, **1**, 1296-1302.
- X. Y. Li, G. H. Chen, Y. Po-Lock and C. Kotal, *Journal of Chemical Technology and Biotechnology*, 2003, **78**, 1246.
- B. N. Zope and R. J. Davis, *Green Chem.*, 2011, **13**, 3484.
- S. Yurdakal, G. Palmisano, V. Loddo, V. Augugliaro and L. Palmisano, *Journal of the American Chemical Society*, 2008, **130**, 1568.
- D. Tsukamoto, Y. Shiraishi, Y. Sugano, S. Ichikawa, S. Tanaka and T. Hirai, *Journal of the American Chemical Society*, 2012, **134**, 6309.
- Y. H. Shen, S. H. Zhang, H. J. Li, Y. Ren and H. C. Liu, *Chemistry-A European Journal*, 2010, **16**, 7368.
- Y. Kwon and M. T. M. Koper, *ChemSusChem*, 2013, **6**, 455.
- Y. N. Jin, G. H. Zhao, M. F. Wu, Y. Z. Lei, M. F. Li and X. P. Jin, *The Journal of Physical Chemistry C*, 2011, **115**, 9917.
- S. N. Chai, G. H. Zhao, P. Q. Li, Y. Z. Lei, Y. N. Zhang and D. M. Li, *The Journal of Physical Chemistry C*, 2011, **115**, 18261.
- P. Q. Li, G. H. Zhao, X. Cui, Y. G. Zhang and Y. T. Tang, *J. Phys. Chem. C*, 2009, **113**, 2375.
- G. H. Zhao, Y. Z. Lei, Y. G. Zhang, H. X. Li and M. C. Liu, *J. Phys. Chem. C*, 2008, **112**, 14786.
- P. Li, Y. Xin, Q. Li, Z. P. Wang, Z. L. Zhang and L. Zheng, *Environmental science & technology*, 2012, **46**, 9600.
- J. Beckers and G. Rothenberg, *Green Chemistry*, 2010, **12**, 939.
- B. T. Kusema and D. Y. Murzin, *Catalysis Science & Technology*, 2013, **3**, 297.
- C. D. Pina, E. Falletta and M. Rossi, *Chemical Society Reviews*, 2012, **41**, 350.
- B. H. Wu and N. F. Zheng, *Nano Today*, 2013, **8**, 168.
- P. Rodriguez, Y. Kwon and M. T. M. Koper, *Nature chemistry*, 2012, **4**, 177.
- A. Primo, T. Marino, A. Corma, R. Molinari and H. Garcia, *Journal of the American Chemical Society*, 2011, **133**, 6930.
- Y. L. Xie, Z. X. Li, Z. G. Xu and H. L. Zhang, *Electrochemistry Communications*, 2011, **13**, 788.
- H. Wen, Z. F. Liu, Q. B. Yang, Y. X. Li and J. Yu, *Electrochimica Acta*, 2011, **56**, 2914.
- Z. H. Zhang, L. B. Zhang, M. N. Hedhili, H. N. Zhang and P. Wang, *Nano letters*, 2012, **13**, 14-20.
- H. Y. Tian, G.H. Zhao, Y. N. Zhang, Y. B. Wang and T. C. Cao, *Electrochimica Acta*, 2013, **96**, 199.
- Z. L. Wu, M. J. Li, D. R. Mullins and S. T. Overbury, *ACS Catalysis*, 2012, **2**, 2224.
- W. P. Shan, F. D. Liu, H. He, X. Y. Shi, C. B. Zhang, *Catalysis Today*, 2012, **184**, 160.
- J. A. Rodriguez, S. Ma, P. Liu, J. Evans and M. Perez, *Science*, 2007, **318**, 1757.

- 40 M. D. Ye, J. J. Gong, Y. K. Lai, C. J. L and Z. Q. Lin, *Journal of the American Chemical Society*, 2012, **134**, 1572.
- 41 N. Zhang, X. Z. Fu and Y. J. Xu, *Journal of Materials Chemistry*, 2011, **21**, 8152.
- 42 N Zhang, S.Q. Liu, X. Z. Fu and Y. J. Xu, *The Journal of Physical Chemistry C*, 2011, **115**, 22901.

Table of Contents Graphic



Highly efficient visible-light driven synergistic photoelectrocatalytic aerobic oxidation of biomass alcohols to aldehyde using Au/CeO₂-TiO₂ NTs photocathode at the mild condition